Supplemental Experimental procedures

Thermodynamic analysis - Thermodynamic experiments were performed using a Biacore T100 biosensor over a temperature range of 4°C to 40°C. Data were fitted to the integrated non-linear form of van't Hoff equation (Zhukov, A., & Karlsson, R. (2007). Statistical aspects of van't Hoff analysis: a simulation study. *J. Mol. Recognit*. ***20***, 379-385) (Figure S1):

$$lnK_a(T) = lnK_a(T_0) + \left[\frac{-\Delta H(T_0)+\Delta C_p T_0}{R}\right] \times \left(\frac{1}{T} - \frac{1}{T_0}\right) + \frac{\Delta C_p}{R} \times ln\left(\frac{T}{T_0}\right) \qquad (1)$$

where R is the gas constant, T_0 is a reference temperature, commonly 298 K, $K_A(T_0)$ and $\Delta H°(T_0)$ - association binding constant and binding enthalpy at T_0, and $\Delta C°_p$ is a heat capacity increment. In several cases, where the relationship $\ln K_A$ *vs*. 1/T assumed strictly linear form, the heat capacity contribution was virtually equal to zero and the relationship was described by a more simple form of the same equation:

$$lnK_a(T) = lnK_a(T_0) + \left[\frac{-\Delta H(T_0)}{R}\right] \times \left(\frac{1}{T} - \frac{1}{T_0}\right) \qquad (2)$$

Confidence probability of 0.95 was used for fitting. The fitting was performed using Microcal Origin 7 software.

Reporter gene assay - The effect of different ALK1 mutations on BMP9 and BMP10 signaling was evaluated in human glioblastoma T98G cells. Briefly, TG98 cells were co-transfected with pGL3-BRE reporter plasmid containing firefly luciferase gene controlled by SMAD1/5/8 and pRL-CMV-luc plasmid containing Renilla luciferase controlled by a constitutively active CMV promoter at a 20:1 ratio. Cells were incubated for 16 hours at 37°C with BMP9 (600 pg/mL) or BMP10 (350 pg/mL) with or without ALK1 mutants. Cells were lysed, assayed using a Dual-Luciferase reporter assay kit (Promega) and results expressed as a ratio of firefly over Renilla luciferase activity in relative light units.

Cooperativity experiment performed by SPR – $ALK1^{ECD}$-BMP9 complex was formed by mixing BMP9 with $ALK1^{ECD}$-hFc. Pre-assembled complex was captured on anti-hFC IgG Biacore chip. Different concentrations of $ActRIIB^{ECD}$-mFC were injected over captured pre-assembled binary ALK1-BMP9 complex. Kinetic parameters for ActRIIB binding to binary ALK1-BMP9 complex were compared with kinetic parameters of ActRIIB binding to BMP9. In a separate experiment assay was flipped and $ActRIIB^{ECD}$-BMP9 complex was formed by mixing BMP9 with $ActRIIB^{ECD}$-mFC. Assembled binary complex was captured on anti-mFc IgG Biacore chip.

Different concentrations of ALK1^{ECD}-hFc were injected over captured binary ActRIIB-BMP9 complex. Kinetic parameters for ALK1 binding to binary ActRIIB-BMP9 complex were compared with kinetic parameters of ALK1 binding to BMP9.

Supplemental Figures:

Supplemental Figure 1. Van't Hoff plots for (A) BMP9 and (B) BMP10 binding to ALK1^{ECD}-Fc, ActRIIB^{ECD}-Fc and ActRIIA^{ECD}-Fc.

Supplemental Figure 2. Higher order assembly in the ALK1^{ECD}-BMP9-ActRIIB^{ECD} crystal structure Asn^{24} on ActRIIB facilitates dimerization of two ternary complexes via the attached N-acetyl-glucosamine (NAG).

Supplemental Figure 3. Comparison of ALK1 with ALK3 and ALK6 (A) Structure-based sequence alignment of ALK1, ALK3 and ALK6, showing residues involved in ligand recognition. Polar (red) and hydrophobic (grey) contacts are highlighted. (B) Peeled-away surface of ALK1, ALK3 and ALK6 mapping residues involved in ligand recognition (colored as in A).

Supplemental Figure 4. Sequence alignment of BMP9 with select TGF-β ligands. BMP9 residues at the ALK1 and ActRIIB interface are highlighted. Asterisks denote key specificity determinants.

Supplemental Figure 5. The ActRIIB/BMP9 interface. Interactions within (A) the conserved ActRIIB hydrophobic binding pocket and (B) surrounding interface are highlighted.

Supplemental Figure 6. Binding of type I and type II receptor ECDs in ALK1-BMP9-ActRIIB complex is independent. To measure possible cooperativity binding of ActRIIB^{ECD} to pre-assembled ALK1^{ECD}-BMP9 binary complex (A) was compared to binding of ActRIIB^{ECD} to BMP9 (B). Assay was flipped and binding of ALK1 to pre-assembled ActRIIB^{ECD}-BMP9 complex (C) was compared to binding of ALK1^{ECD} to BMP9 (D).

Supplemental Tables:

Supplemental Table 1: Crystallographic data collection and refinement statistics.

Supplemental Table 2: Interactions at the ALK1/BMP9 interface.

Supplemental Table 3: Interactions at the ActRIIB/BMP9 interface.

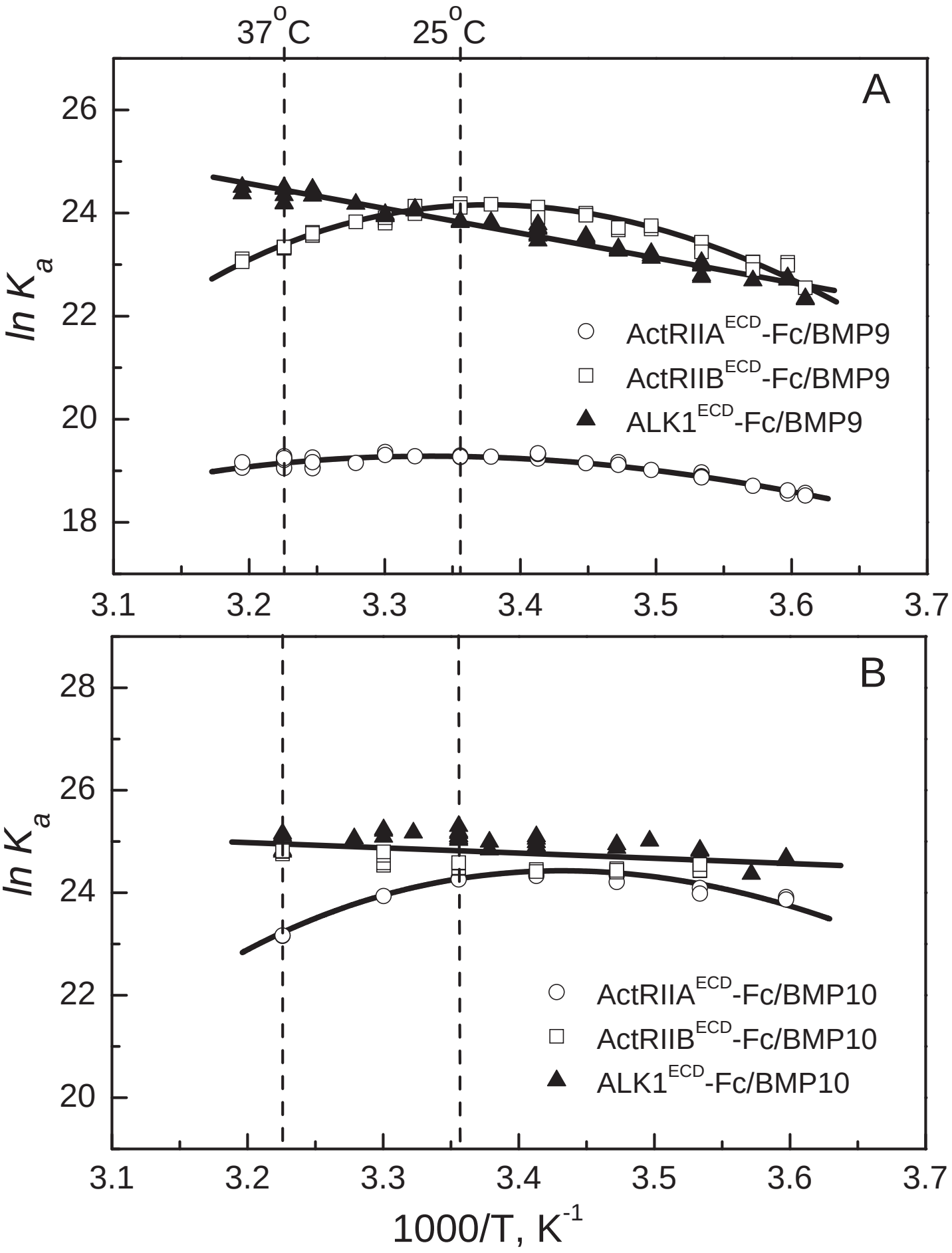

Supplemental Figure 1

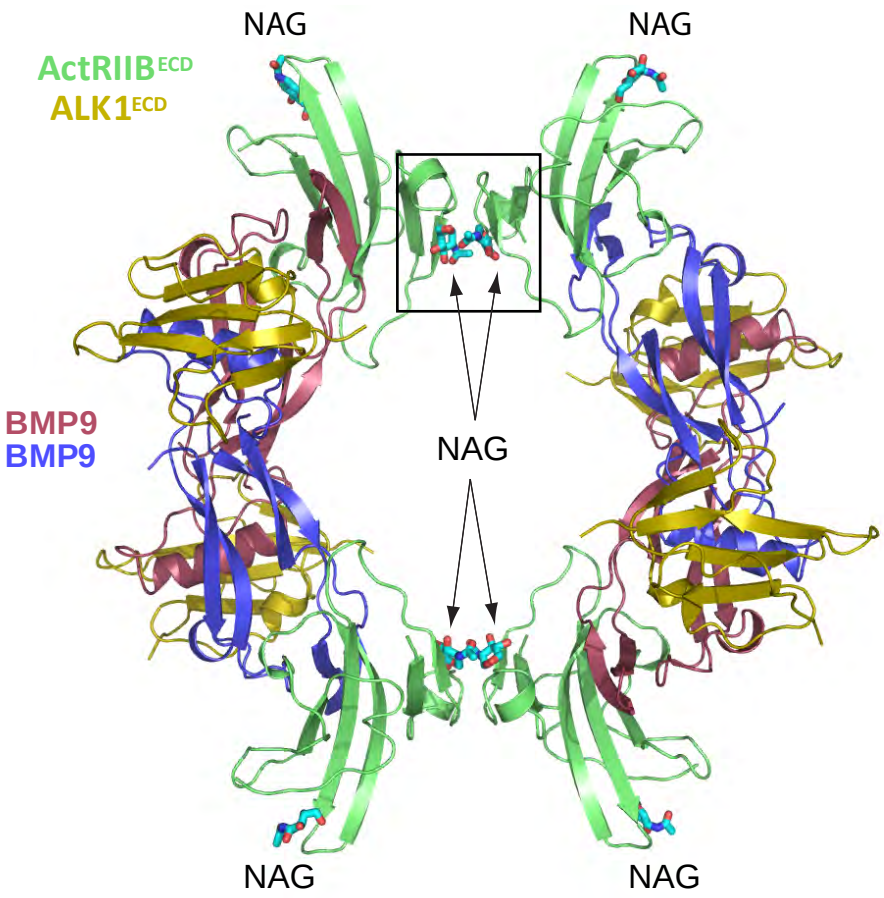

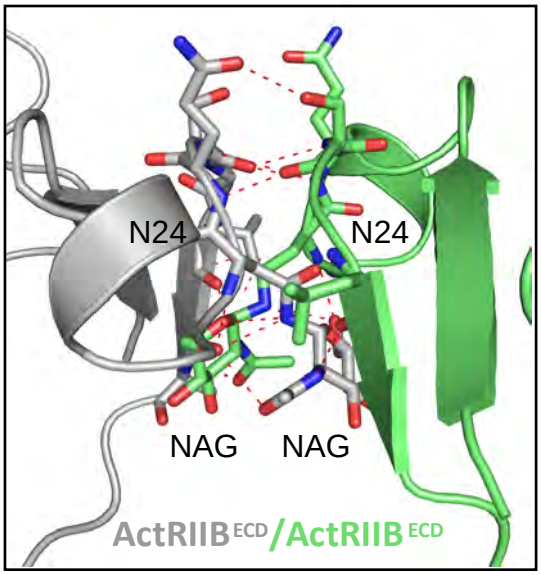

Supplemental Figure 2

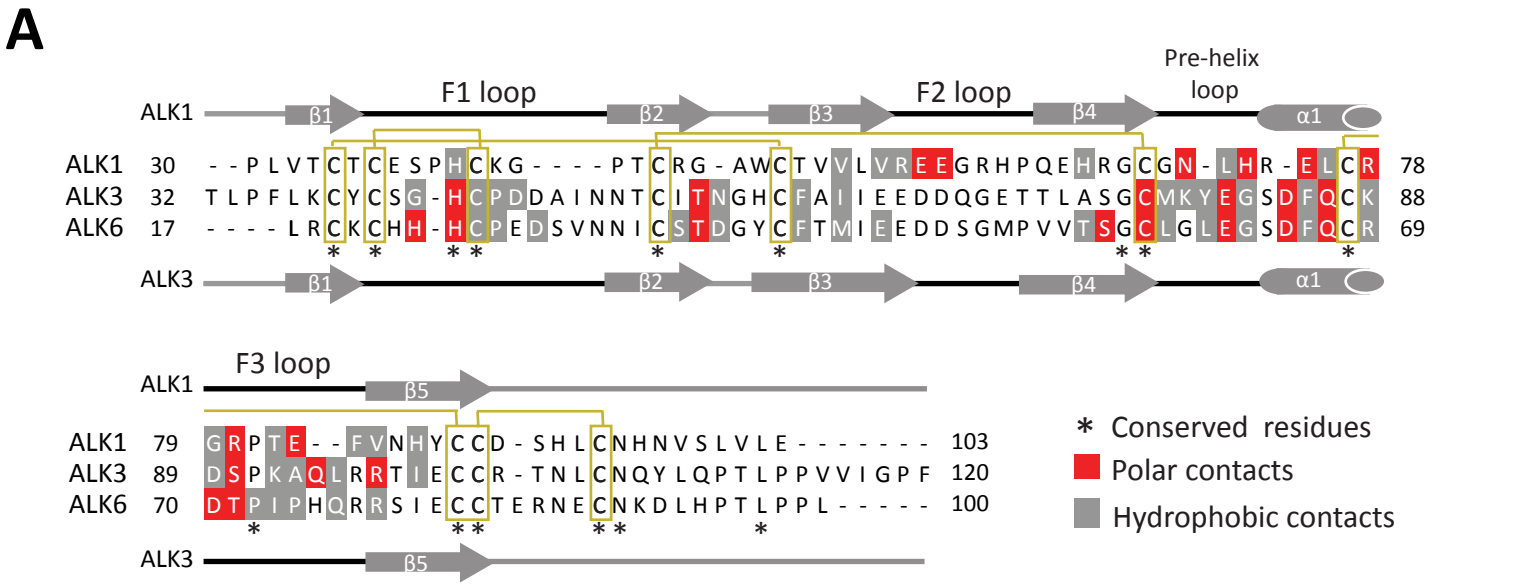

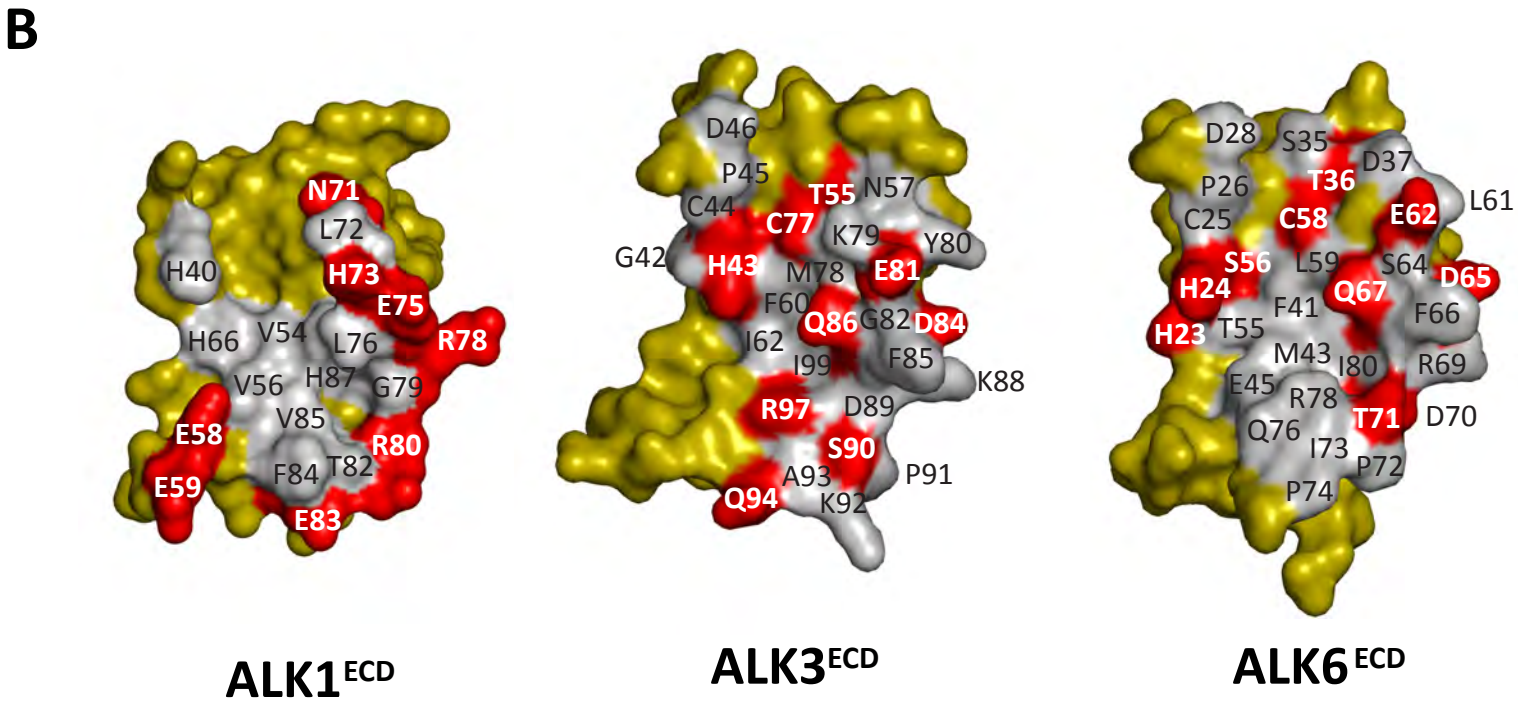

Supplemental Figure 3

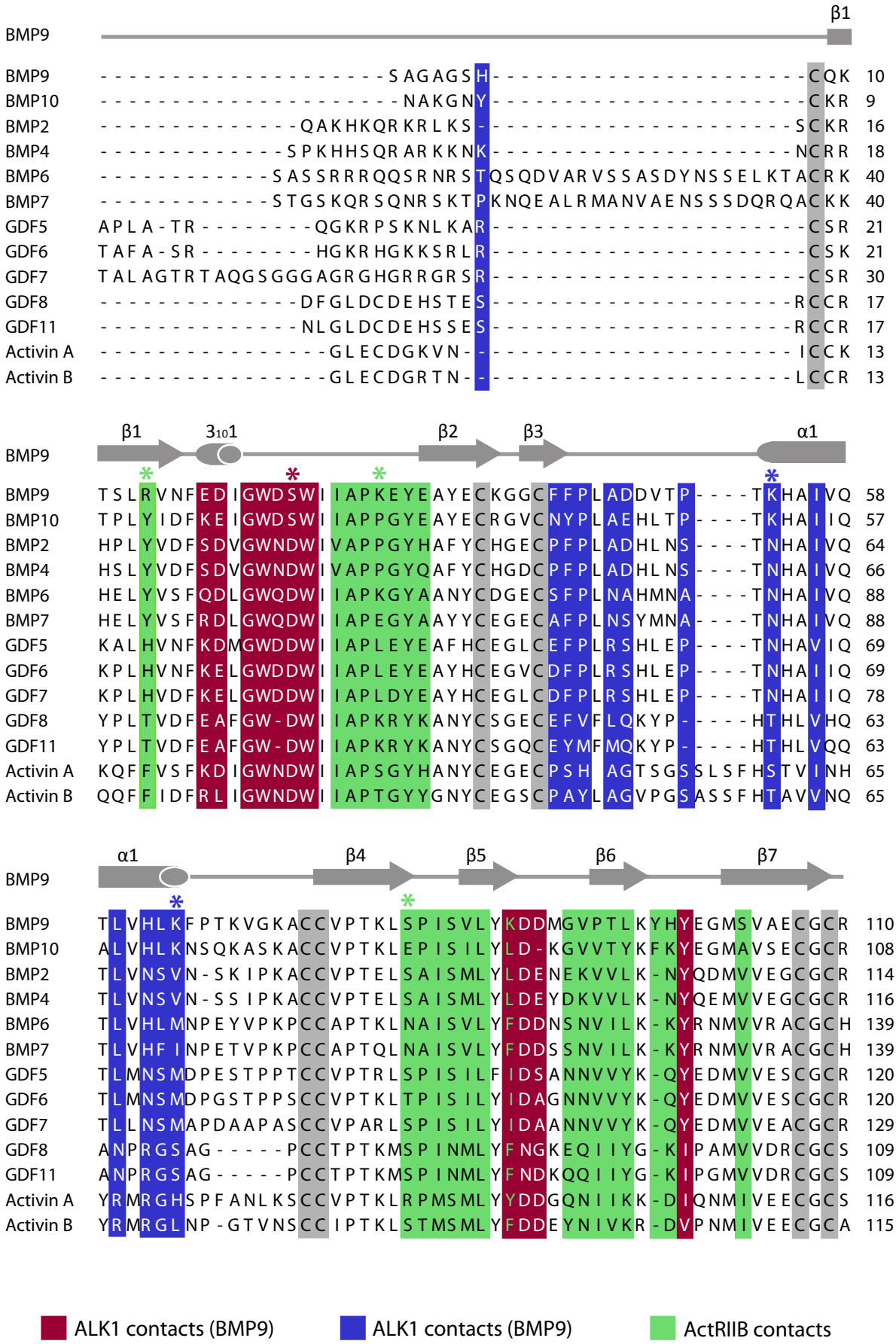

Supplemental Figure 4

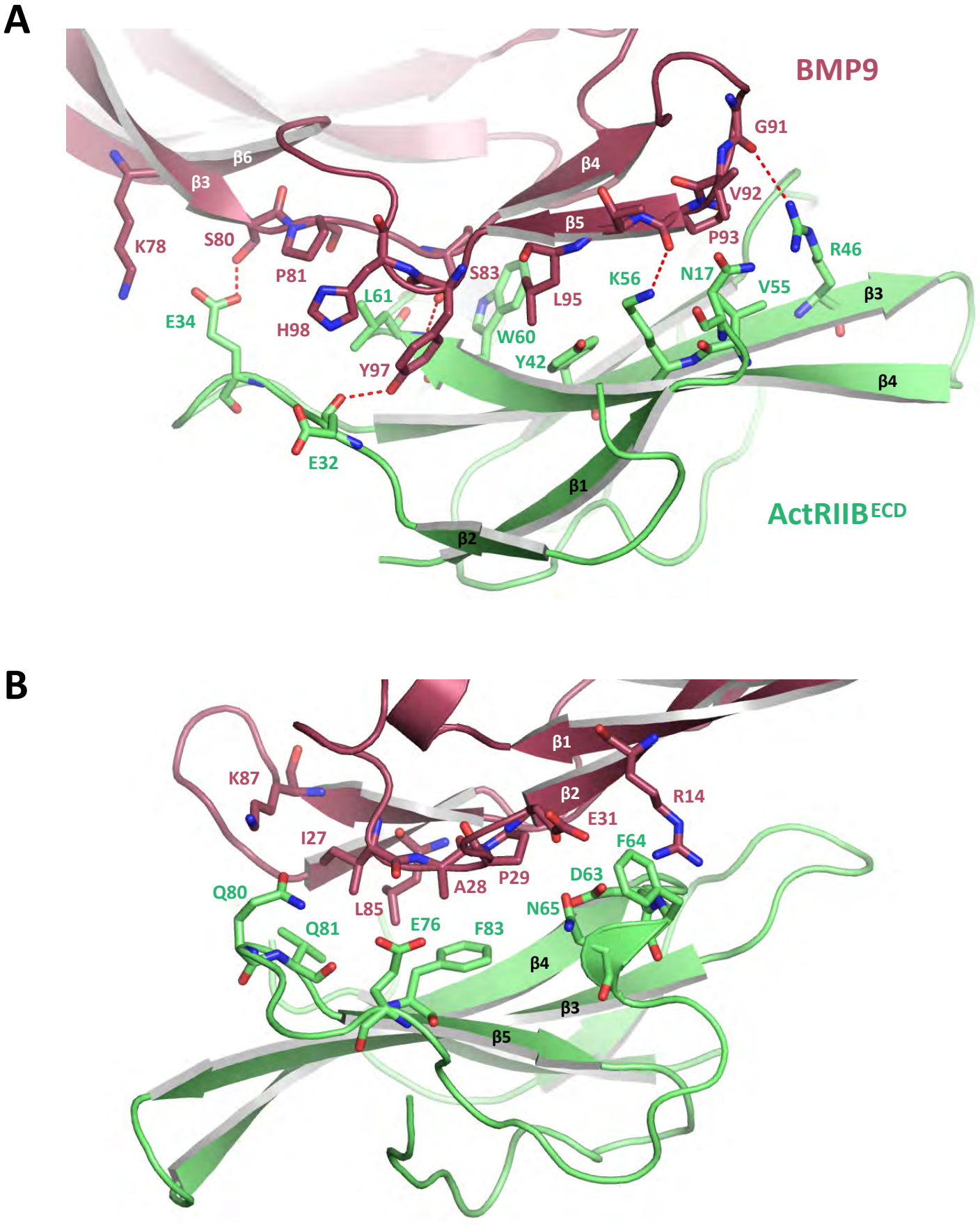

Supplemental Figure 5

A

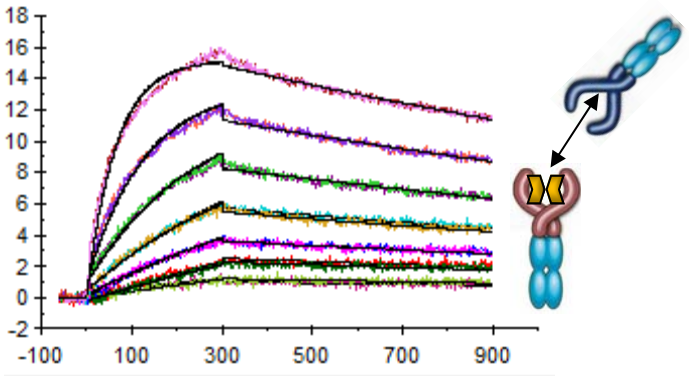

k_a = 3.74 x 10^6 ($M^{-1}s^{-1}$)

k_d =4.42 x 10^{-4} (s^{-1})

K_D = 118 pM

B

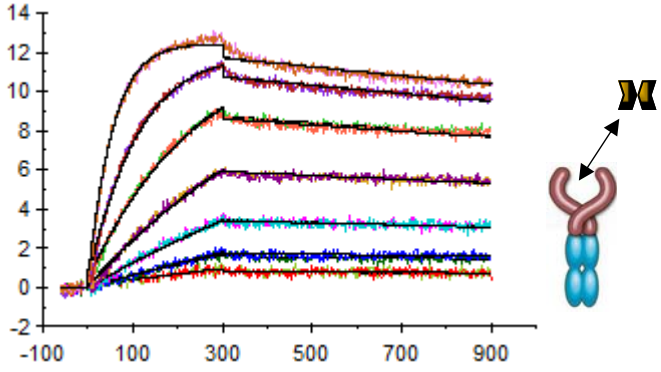

k_a = 4.27 x 10^6 ($M^{-1}s^{-1}$)

k_d = 2.10 x 10^{-4} (s^{-1})

K_D = 49 pM

C

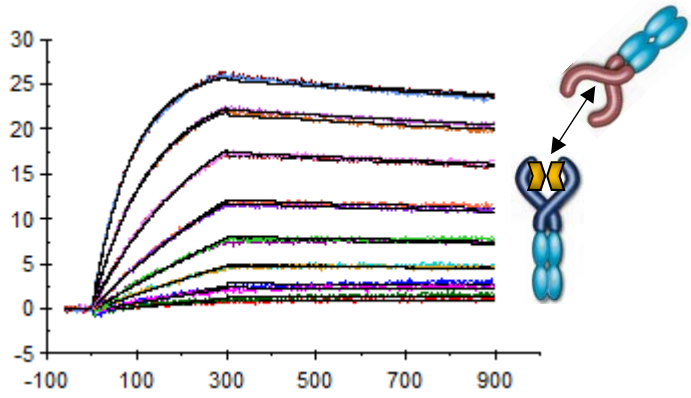

k_a = 7.35 x 10^5 ($M^{-1}s^{-1}$)

k_d =1.28 x 10^{-4} (s^{-1})

K_D = 175 pM

D

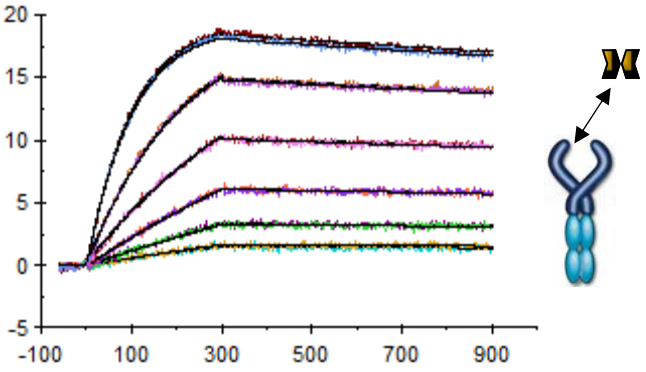

k_a = 2.24 x 10^6 ($M^{-1}s^{-1}$)

k_d = 1.29 x 10^{-4} (s^{-1})

K_D = 58 pM

Supplemental Figure 6

Supplemental Table 1: Crystallographic Data

Data collection Statistics	
Space group	$P3_112$
Cell dimensions	
a, *b*, *c* (Å)	216.45, 216.45, 216.95
α, β, γ (°)	90.00, 90.00, 120.00
Wavelength (Å)	1.54
Resolution (Å)	26.8- 3.35 (3.41-3.35)
R_{merge}	0.137 (0.372)
$I / \sigma I$	20.9 (4.7)
Completeness (%)	99.5 (99.4)
Redundancy	5.8 (3.9)
Refinement Statistics	
Resolution (Å)	26.8 -3.35
No. of Reflections	69520
R_{work}/R_{free}	21.9/26.1
Average B ($Å^2$)	78
Rmsd bond lengths (Å)	0.014
Rmsd bond angles (°)	1.2

Numbers in parentheses correspond to highest resolution shell
$R_{merge} = \Sigma |I - \langle I \rangle| / \Sigma \langle I \rangle$
$R_{work} = \Sigma ||F_{obs}| - |F_{calc}|| / \Sigma |F_{obs}|$ where F_{obs} and F_{calc} are the observed and calculated structure factors respectively.
R_{free} was calculated from a subset of reflections (5%) not used for refinement.

Supplemental Table 2: Interactions (d ≤ 4.5 Å) at the BMP9/ALK1 interface

BMP9/ALK1 Site I

ALK1	BMP9
His40	His7, Ala46
Val54	Phe43, Pro44
Val56	Phe43, Leu63
Arg57	Leu63
Glu58	**Phe42,** Phe43, His62 Leu63
Glu59	Phe42,His62, Leu63, **Lys71**
His66	Pro44
Asn71	**Asp47**
Val80	Phe43
His87	Phe43, Pro44

BMP9/ALK1 Site II

ALK1	BMP9
Arg78	Ser24, Trp25, **Lys87, Asp88, Asp89**
Gly79	Gly21
Arg80	**Glu18, Gly21, Asp23**
Thr82	Asp19, Gly21
Glu83	Asp19, **Lys64**
Phe84	Asp19, Lys64

BMP9/ALK1 Site III

ALK1	BMP9
Leu72	Asp47, Pro51
His73	**Pro51,** Lys53, Ile56
Glu75	**Lys53,** Trp22, Trp25 **Tyr99**
Leu76	Phe43, Ile56, Leu60 Trp22

BMP9 Residues highlighted in bold are involved in polar contacts

Supplemental Table 3: Interactions (d ≤ 4.5 Å) at the BMP9/ActRIIB interface

BMP9/ActRIIB		BMP9/ActRIIB	
ActRIIB	**BMP9**	**ActRIIB**	**BMP9**
Asn17	Val92	Lys56	**Pro93**, Thr94, Leu95
Glu21	Thr94	Cys59	Leu95, Tyr97
Cys31	Tyr97	Trp60	Ala28, Pro29, Ser83, Val84, Leu85, Leu95
Glu32	**Tyr97**, His98	Leu61	Pro81, Ile82,**Ser83**, Tyr97**,** His98
Glu34	**Lys78**, **Ser80**, Pro81, Ala105	Asp63	Pro29
Lys37	Ser80, Pro81, Ser103	Phe64	Arg14, Glu31,Tyr32, Glu33
Leu39	Tyr97	Asn65	Pro29, Glu31
Tyr42	Leu85, Leu95	Glu76	Lys30
Ser44	Leu85	Gln80	Ile27, Lys30, Lys87
Arg46	**Gly91**, Pro93	Val81	Ile27, Pro93
Val55	Pro93	Phe83	Ile27, Ala28, Leu85

BMP9 Residues highlighted in bold are involved in polar contacts